

3.1 General Principles of Raman Spectroscopy

Raman scattering is the process of inelastic light scattering that occurs on fluctuations in the polarizability of molecules which are excited to higher vibrational or rotational energy levels. This phenomenon was discovered in 1928 by C.V. Raman and K.S. Krishnan (for liquids) and L.I. Mandelshtam and G.S. Landsberg (for crystals).

In Raman scattering, a monochromatic line of exciting laser radiation after interaction with a substance is accompanied by an additional set of spectral components. The newly appeared lines are located on the scale of electromagnetic waves symmetrically with respect to the line of exciting radiation and are separated from it by the frequencies of atomic vibrations. The totality of newly emerging spectral components is the Raman spectrum of a substance, which is its diagnostic feature. The phenomenon of Raman scattering is characteristic of substances that are in a gaseous, liquid, or solid state consisting of molecules or molecular complexes with an internal structure, or atoms combined into crystalline structures. Monatomic gas particles that do not interact with each other (for example, inert gases) do not have Raman spectra.

The source of secondary radiation (Raman scattering) is a variable in time electric dipole moment that occurs in the medium as a result of the interaction of particles of a substance with the electric component of external electromagnetic radiation of the visible or close to visible range. The magnitude of the dipole moment depends on the magnitude of the external field and on the polarizability of the substance:

$$\mathbf{p} = \hat{\alpha}\mathbf{E}$$

where \mathbf{p} is the induced electric dipole moment vector, \mathbf{E} is the vector of external electric field strength, and $\hat{\alpha}$ is the polarizability.

The polarizability of the substance depends on the structure of the molecules or crystals forming it, on the types of bonds in the substance, as well as on the nature of the motions of the atoms in the molecules or in the crystals. Polarizability is a variable in time characteristic of the substance, which is modulated by the movements of the particles of the substance itself and the electrical component of the external electromagnetic field, causing the appearance of a variable electric dipole moment in the substance. In accordance with the basic rule of electrodynamics, a system with a variable electric dipole moment in time can

be a source of electromagnetic radiation with a frequency of change in the dipole moment.

In experiments on Raman scattering using monochromatic radiation with a frequency of Ω , spectral components with frequencies Ω , $(\Omega + \omega_i)$ and $(\Omega - \omega_i)$ are recorded in the spectrum of scattered radiation, where ω_i are the frequencies of vibrational and rotational motions of particles of a substance. The spectral region in which the components are located with frequencies greater than the frequency of laser radiation $(\Omega + \omega_i)$ is commonly called the anti-Stokes region, and the region with lower frequencies $(\Omega - \omega_i)$ is called the Stokes region.

Under normal conditions, the intensity of the strongest lines in the Stokes region of the Raman spectra is usually 10^{-6} – 10^{-8} of the intensity of the exciting line (Reshetnyak and Bukanov 1991). The intensity of the anti-Stokes component is even less by several decimal exponents of magnitude and decreases rapidly with increasing magnitude of the detuning from the laser line. For this reason, the bulk of the experiments are carried out in the Stokes spectral region. As a source of spectral information, mainly vibrational spectra are used.

Polarizability is anisotropic and is described by a second rank tensor, which can be written as a symmetric matrix:

$$\hat{a} = \begin{vmatrix} a_{xx} & a_{xy} & a_{xz} \\ a_{yx} & a_{yy} & a_{yz} \\ a_{zx} & a_{zy} & a_{zz} \end{vmatrix}$$

The component of the polarizability tensor a_{ij} determines the magnitude of the dipole moment arising in the medium along the i axis under the action of an electromagnetic field with the direction of the polarization vector of the electric field along the j axis. This means that for different orientations of the polarization vector of the laser radiation and the polarization vector of the detected scattered radiation in the Raman spectrum, scattering will be recorded on different components of the polarizability tensor. In a general case, Raman scattering occurs at different vibrations, and the recorded scattering lines in the Raman spectra have different frequencies

and intensities. The intensity of the scattering line in the case of nonpolar normal vibrations is determined by the following formula:

$$I \sim \left[\sum f_i \alpha_{ij} e_j \right]^2, \\ i, j = x, y, z$$

where f_i and e_j are components of the unit vectors of the dipole moment polarization and laser radiation, respectively, and α_{ij} is the change of the polarizability tensor component at a given kind of normal vibrations. Not all types of vibrations can be detected as lines in the Raman spectra. For molecules and crystals with an inversion center, there is an alternative prohibition rule which is very important for experimental practice. According to this rule, for compounds with an inversion center, bands of antisymmetric (with respect to the inversion center) vibrations are forbidden in the Raman spectra, and symmetrical ones are forbidden in the IR spectra. The alternative prohibition rule relates simultaneously to Raman spectroscopy and IR absorption spectroscopy and indicates the complementary nature of these methods of molecular spectroscopy.

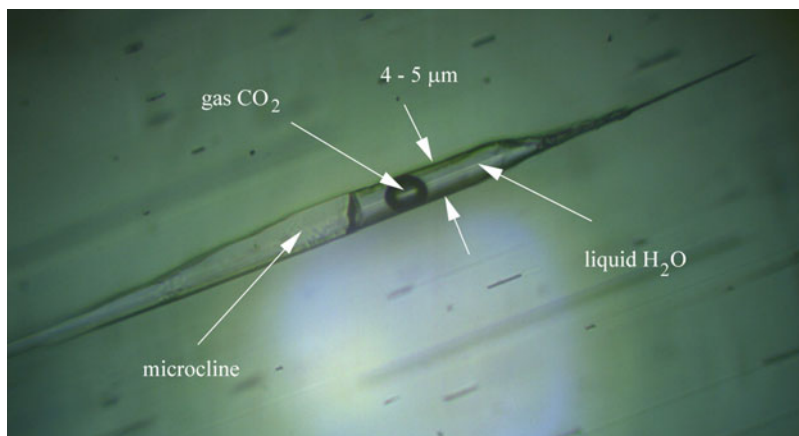
The theory of Raman spectroscopy is described in more detail in numerous publications (Brandmüller and Moser 1962; Anderson 1973; Sushchinsky 1981; Banwell 1983; Zhizhin et al. 1984; Nakamoto 2009).

3.2 Specific Features and Possibilities of Raman Spectroscopy: Practical Recommendations

3.2.1 Advantages and Disadvantages of the Method

The most important properties of Raman spectroscopy are that this method is nondestructive and local. The ability of laser radiation to penetrate inside transparent minerals makes Raman spectroscopy indispensable for diagnosing mineral phases in inclusions (see, e.g., Figs. 3.1 and 3.2). In this case, the minimum dimensions of the

Fig. 3.1 A three-phase inclusion in aquamarine. The transverse size of the inclusion is about 4–5 μm



investigated phases are limited by the diameter of the focal spot of laser radiation. When using high-quality optical elements, laser radiation can be focused into a spot with a diameter of up to several microns. In this case, phase diagnostics can be carried out in situ, without damage the inclusions and disbalance the phase equilibrium. The highest quality Raman spectra are obtained for solid-state phases because of their high density (Fig. 3.3).

Figure 3.2 illustrates both the large diagnostic capabilities of Raman spectroscopy and the difficulties encountered in the study of inclusions. Laser radiation, before it reaches an inclusion, goes some distance in the host mineral causing Raman scattering in the latter. As a result, the resulting spectrum contains the scattering lines

of both the studied inclusion and the host mineral. In the cases when the host mineral spectrum is rich in its own scattering lines, the diagnosis of the substances of microscopic inclusions can be significantly complicated. It should be taken into account that in the spectra of microscopic inclusions usually only most intense scattering lines can be observed, which may have low intensities against the background of the more powerful spectrum of the host mineral. Obtaining spectra of inclusions located as close as possible to the surface of the host mineral reduces the laser beam path through the latter. The depth at which diagnostics of inclusions is possible is limited by the focal length of the lens used.

In some cases, in multiphase inclusions, it is possible to diagnose not only solid, but also liquid (Fig. 3.4) and gaseous (Figs. 3.5 and 3.6) phases.

In the region of stretching vibrations of water, a strong and narrow scattering line with a frequency of 3610 cm^{-1} is recorded, which refers to H_2O molecules located in the channels of the aquamarine structure. Due to the small diameter of the channels (about 0.5 nm), water molecules exist in a constrained state with hydrogen atoms attached to the channel walls and do not form strong hydrogen bonds. This is reflected in the small half-width of the scattering line of about 4 cm^{-1} . The broad band at 3420 cm^{-1} with a shoulder at 3250 cm^{-1} corresponds to O–H-stretching vibrations of water molecules forming rather strong hydrogen bonds and belonging to the liquid phase of the inclusion.

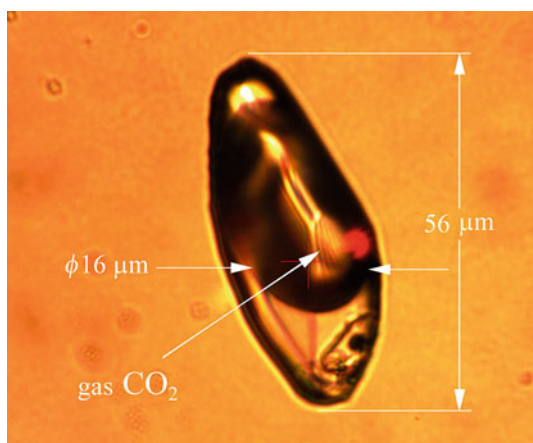


Fig. 3.2 A multiphase inclusion in topaz

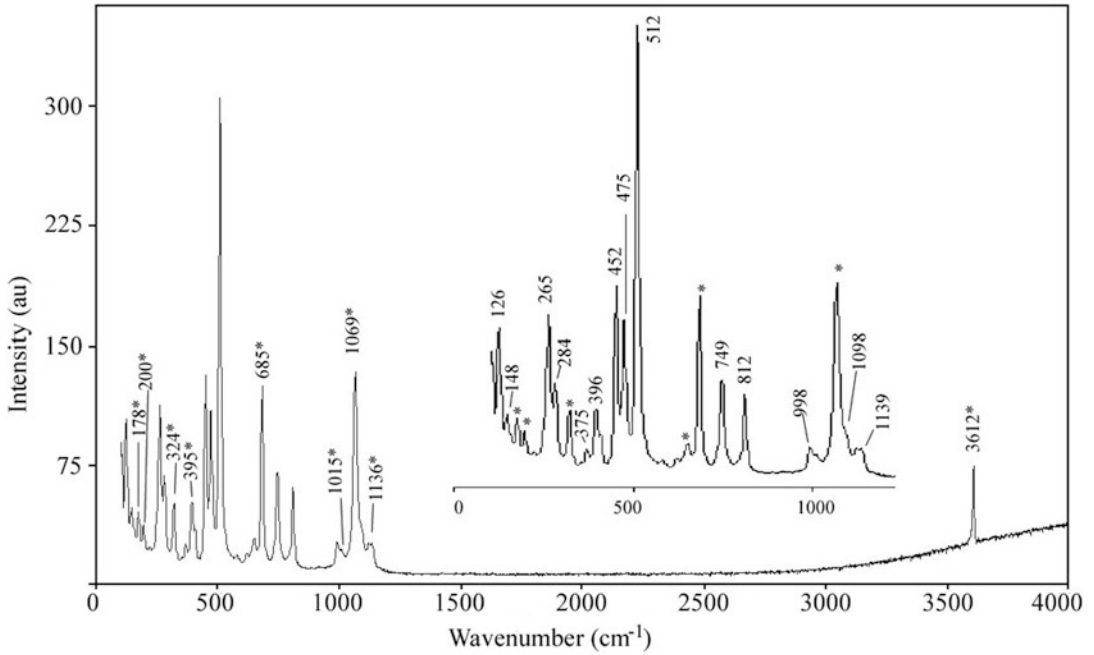


Fig. 3.3 Raman spectrum of a microscopic inclusion of microcline in aquamarine. Bands marked with an asterisk belong to the aquamarine matrix. The laser emission wavelength is 532 nm, the spectral resolution is about 6 cm^{-1} , and the laser power is 30 mW

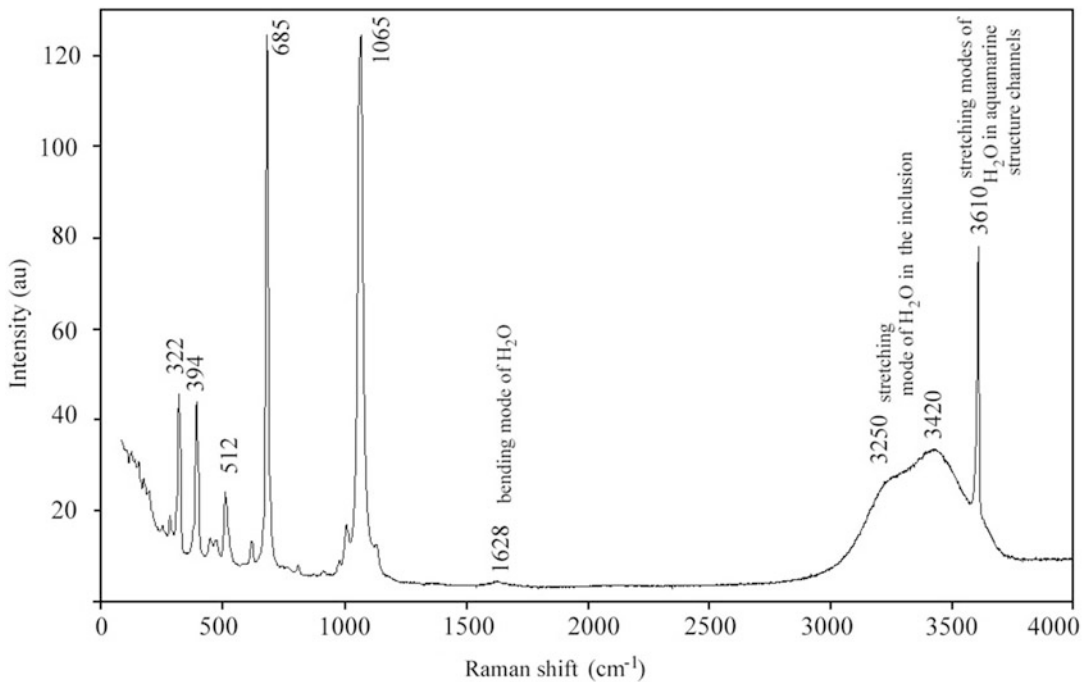


Fig. 3.4 Raman spectrum of the liquid phase of the inclusion in aquamarine

Fig. 3.5 Raman spectrum showing weak bands of gaseous CO₂ (gas bubble in the liquid) in the inclusion in aquamarine. All strong narrow bands correspond to aquamarine matrix

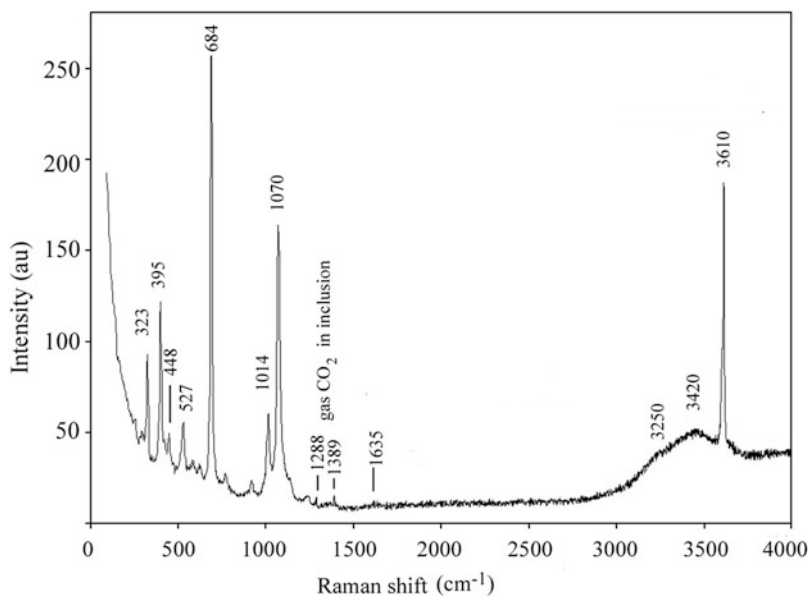
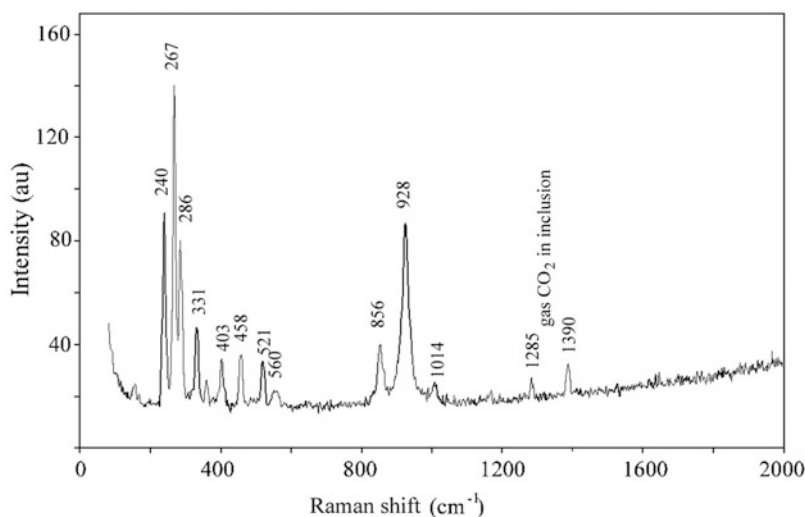


Fig. 3.6 Raman spectrum showing bands of gaseous CO₂ in a multiphase inclusion in topaz (see Fig. 3.2)



To obtain the maximum possible intensity of the Raman signal, the focal volume of the laser beam must be immersed in the substance of the host mineral and pointed at the object under investigation. In this case, a defocused luminous spot forms on the surface of the host mineral at the entry point of the laser beam, which can cover the working field. In such a situation, it is not possible to determine not only the diameter of the focal spot on the phase being diagnosed, but it is also

generally difficult to understand whether the laser beam is focused on the inclusion. In this case, one can judge the success of the experiment only from the results of a comparison of the Raman spectra obtained in the pure region of the host mineral and the spectra obtained from inclusions. Reliable confirmation of the result in this situation is the reproducibility of spectral data.

Another difficulty in working with inclusions is a significant loss of laser power when passing

Fig. 3.7 Sword-like microcrystals of the rare mineral katiarsite $\text{KTiO}(\text{AsO}_4)$ on arsmirandite crystal crust. SEM image (in secondary electrons)

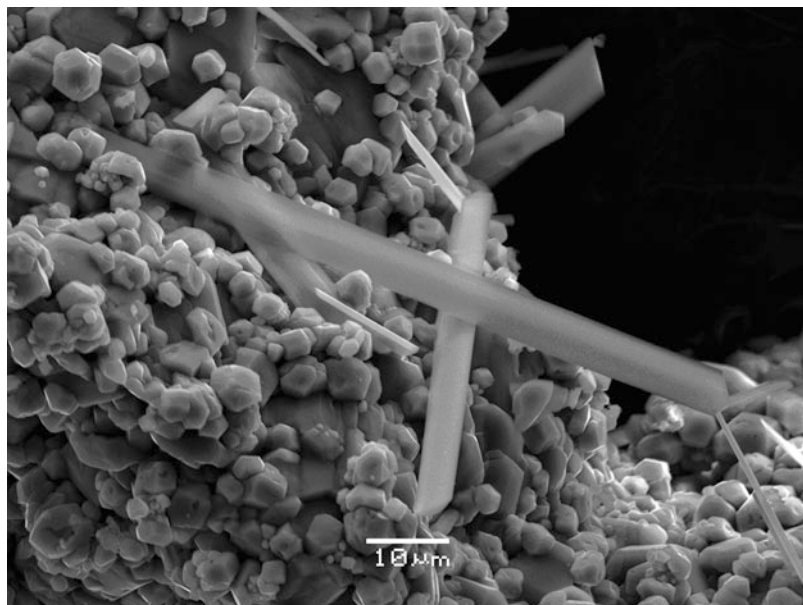
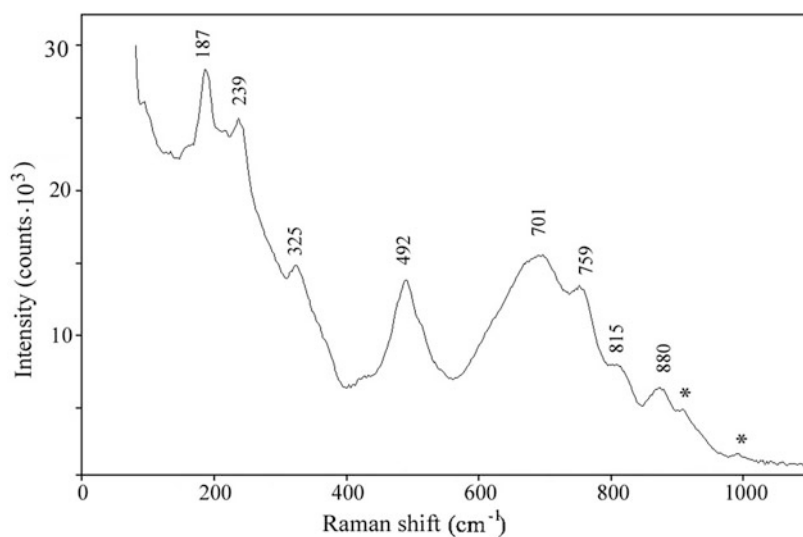


Fig. 3.8 Raman spectrum of katiarsite. A weak band near 1000 cm^{-1} corresponds to an admixed sulfate. The laser emission wavelength is 532 nm , the spectral resolution is about 6 cm^{-1} and the laser power is 30 mW , and the focal spot diameter is $3\text{ }\mu\text{m}$



through the boundary of the inclusion. Uneven boundary can cause strong scattering of the laser beam, reducing the effective exciting power. Moreover, the total internal reflection conditions for a laser beam can be realized on the surface of the inclusion capsule. In this case, the laser beam will not penetrate into the inclusion, and obtaining a Raman spectrum will not be possible.

The “nondestructiveness” and locality of the Raman spectroscopy method were the reason for its widespread use in the study of unique minerals represented by single finds or microscopic monomineral aggregates. If the studied mineral is represented by individual prismatic crystals or thin needles (Fig. 3.7), then to obtain the Raman spectrum (Fig. 3.8), the sample area was chosen

whose linear dimensions are larger than the diameter of the laser beam focal spot. Otherwise, there will be a loss of power of the exciting radiation and the Raman scattering signal.

The intensity of the scattered radiation depends on the number of scattering centers in the focal volume of the laser beam. Therefore, *ceteris paribus*, the best quality of the Raman spectrum will be obtained in the area of the sample where the mineral aggregate has the highest concentration of the substance. For example, with needle-like or finely prismatic microcrystal forms, the Raman spectrum should be recorded at the common base of needle growth. The interpretation of the Raman spectra obtained on the microaggregates of minerals and the identification of the scattering lines related to the mineral of interest require special attention and analysis. When working with microscopic aggregates of minerals, one should take into account the possible presence of mineral impurities, the removal of which is impossible due to the small size.

3.2.2 Spectral Band Assignment

Raman spectra primarily reflect the features of the anionic part of the mineral, as well as some polyatomic cations like NH_4^+ or UO_2^{2-} . The

frequencies of symmetric stretching vibrations of some complex anions occurring in the structures of minerals change mainly in the following ranges (cm^{-1}):

Nesosilicates	820–980	Sulfates	970–1020
Carbonates	1050–1100	Arsenates	800–900
Molybdates	780–880	Tungstates	850–920
Orthophosphates	930–990	Orthovanadates	820–880

Raman shifts of the stretching vibration bands increase with increasing of polymerization of coordination polyhedra; e.g., for Al-poor framework silicates they are typically in the range $1040\text{--}1130\text{ cm}^{-1}$.

Thus, scattering lines observed in these ranges can be used for a preliminary assignment of a mineral to one or more class of compounds as a step preceding a more precise specification. When conducting diagnostic studies, it is necessary to take into account that the approximate proportion of the intensities of the Raman lines in the spectra of complex anions is as follows: MoO_4^{2-} ($\approx \text{WO}_4^{2-}$): SO_4^{2-} : PO_4^{2-} : CO_3^{2-} : SiO_4^{4-} = 10 : 6 : 3 : 1.5 : 1 (for excitation radiation with a wavelength between 488 and 515 nm). This feature can be illustrated by the spectra of cancrinite $\text{Na}_6\text{Ca}_2[\text{AlSiO}_4]_6(\text{CO}_3)_2 \cdot 2\text{H}_2\text{O}$ (Fig. 3.9) and vishnevite $\text{Na}_8[\text{AlSiO}_4]_6(\text{SO}_4) \cdot 2\text{H}_2\text{O}$ (Fig. 3.10), structurally related tectosilicates with additional

Fig. 3.9 Raman spectrum of cancrinite

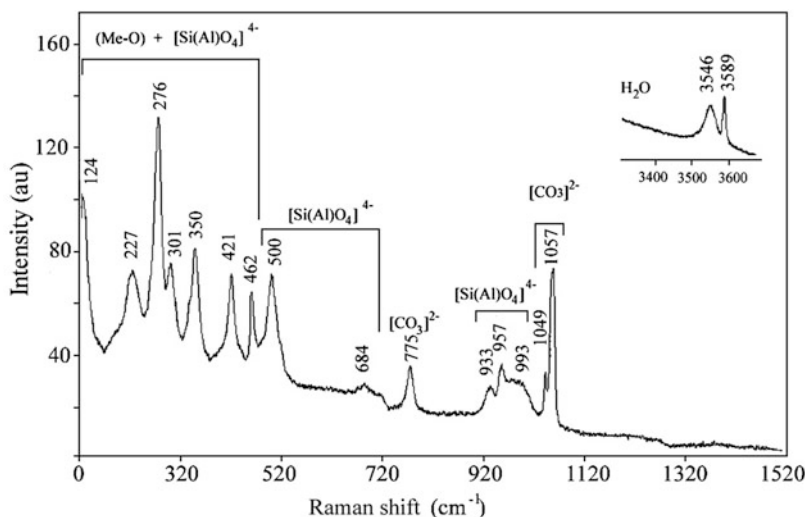
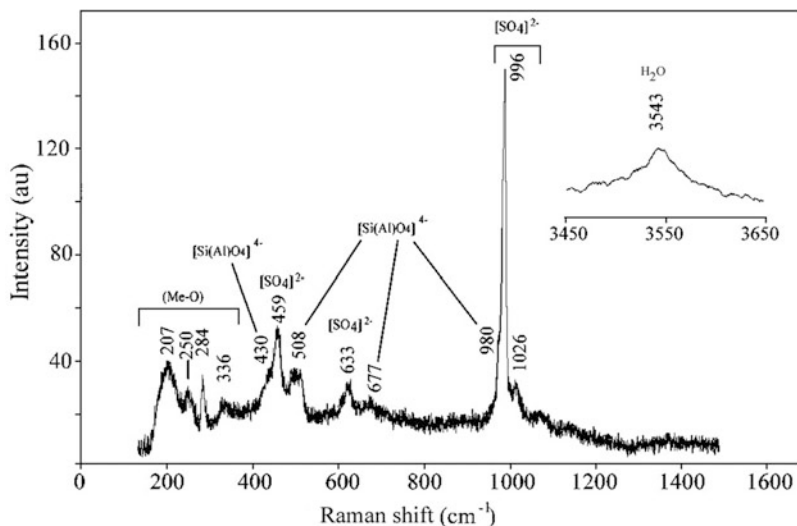


Fig. 3.10 Raman spectrum of vishnevite



anions. The additional anions CO_3^{2-} and SiO_4^{4-} play subordinate role in the chemical composition of these minerals. However, the strongest lines in the Raman spectra are the scattering lines corresponding to the internal fully symmetric stretching vibrations of just additional anions. This feature may cause difficulty in determining chemical class of a mineral.

3.2.3 Effect of Structural Disorder on Raman Spectra of Minerals

It should be noted that Raman spectroscopy is sensitive to the degree of crystallinity of the substance. This is reflected primarily in the half-widths of the scattering lines. Raman spectra of minerals with perfect crystal structures are distinguished by narrow well-resolved bands (Fig. 3.11). Disturbance or absence of long-range order in the structure of matter, cation disordering and local defects cause broadening and even the disappearance of some scattering lines. This effect is most pronounced in the Raman spectra of metamict minerals, minerals with a colloid-dispersed structure, and glasses (Fig. 3.12).

In the spectrum of quartz, narrow clearly defined scattering lines are recorded that belong to different types of vibrations: “rocking of

tetrahedra” (210 cm^{-1}), “twisting of tetrahedra” (353 cm^{-1}), O–Si–O bending (467 cm^{-1}), and Si–O stretching (1086 cm^{-1}) (Ranieri et al. 2009). The absence of a long-range order in obsidian, which is a SiO_2 -rich glass, results in the absence of specific lines corresponding to any symmetry elements. The broad bands at

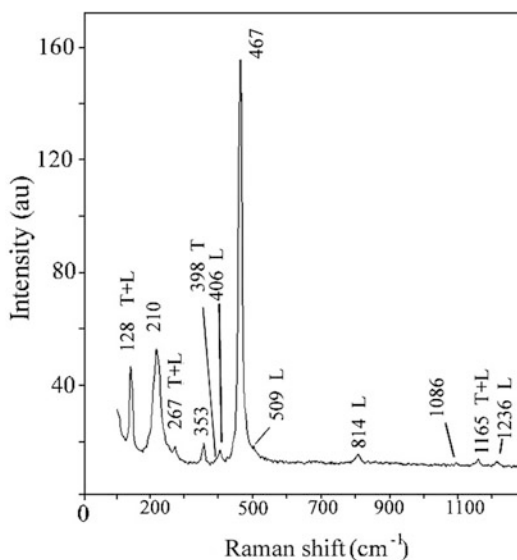


Fig. 3.11 Raman spectrum of quartz powder. The laser emission wavelength is 532 nm, the spectral resolution is 6 cm^{-1} , and the laser power is 30 mW. The letters L and T denote components of longitudinal-transverse splitting (see below)

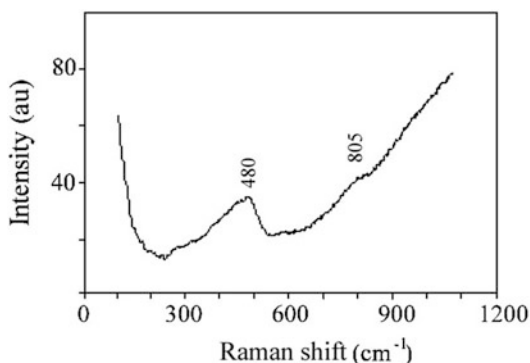


Fig. 3.12 Raman spectrum of obsidian (volcanic glass). The laser emission wavelength is 532 nm, the spectral resolution is 6 cm^{-1} , and the laser power is 30 mW

480 and 805 cm^{-1} correspond to the totality of vibrations in areas with different local structures.

The sensitivity of Raman scattering to the disordered distribution of atoms between crystallographic positions is clearly reflected in the spectra of feldspars. For example, in the structure of the disordered oligoclase $(\text{Na,Ca})[\text{AlSi}_3\text{O}_8]$, Al atoms are statistically distributed between different

tetrahedral sites, whereas in an ordered variety they are concentrated mainly in only one of independent crystallographic positions. Raman spectra of the two oligoclase varieties differ markedly from each other: in the spectrum of an ordered oligoclase variety, a greater number of scattering lines (Fig. 3.13, upper curve) are recorded, which have a smaller half-width than in the spectrum of a disordered oligoclase (Fig. 3.13, lower curve).

In the study of black microscopic inclusions (Fig. 3.14) in aquamarine, it was found [based on the assignment by Sharma et al. (2001)] that they consist of crystalline graphite, which was diagnosed by the relatively narrow line at 1574 cm^{-1} , and X-ray amorphous carbon showing a broad band at 1336 cm^{-1} (Fig. 3.15). The Raman spectrum made it possible to suppose that the substance in the inclusion is compressed, since the frequencies of the recorded scattering lines differ from the values of the frequencies characteristic of the same substances under normal conditions (i.e., 1360 and 1582 cm^{-1} for amorphous carbon and graphite, respectively).

Fig. 3.13 Raman spectra of the ordered (upper curve) and disordered (lower curve) oligoclase varieties. The laser emission wavelength is 532 nm, the spectral resolution is 6 cm^{-1} , and the laser power is 14 mW

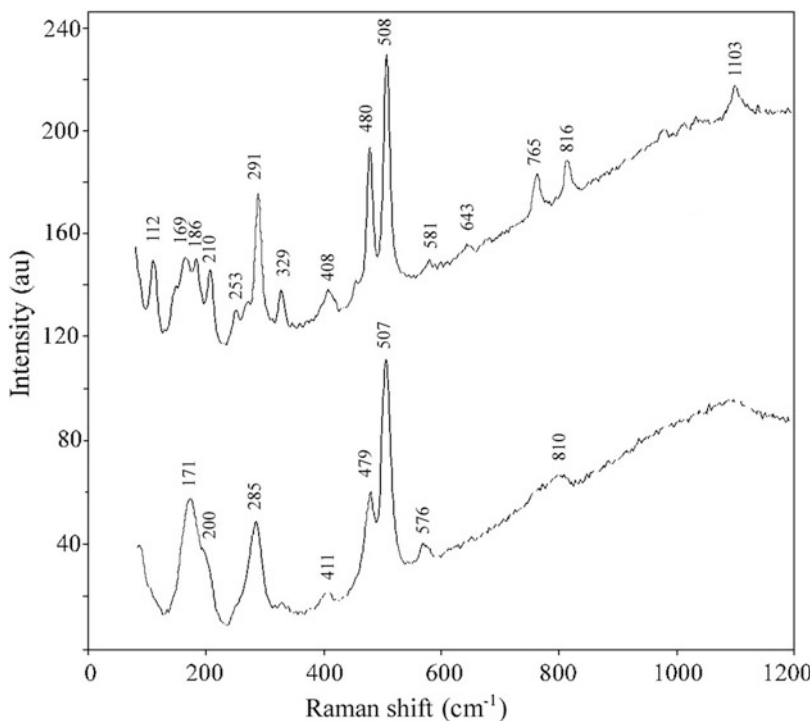


Fig. 3.14 Inclusion of carbonaceous matter in aquamarine

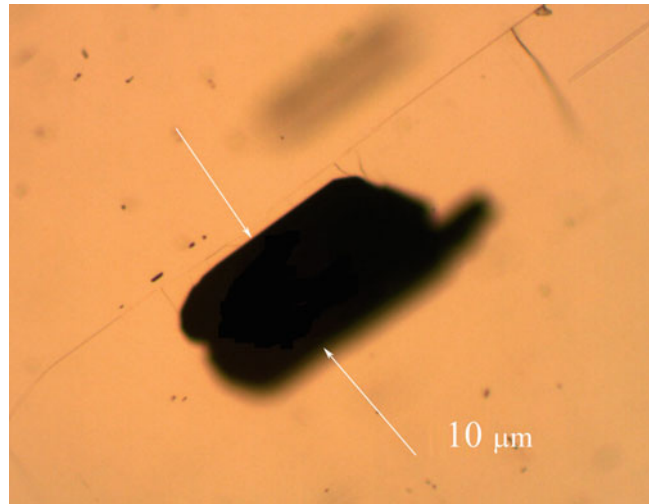
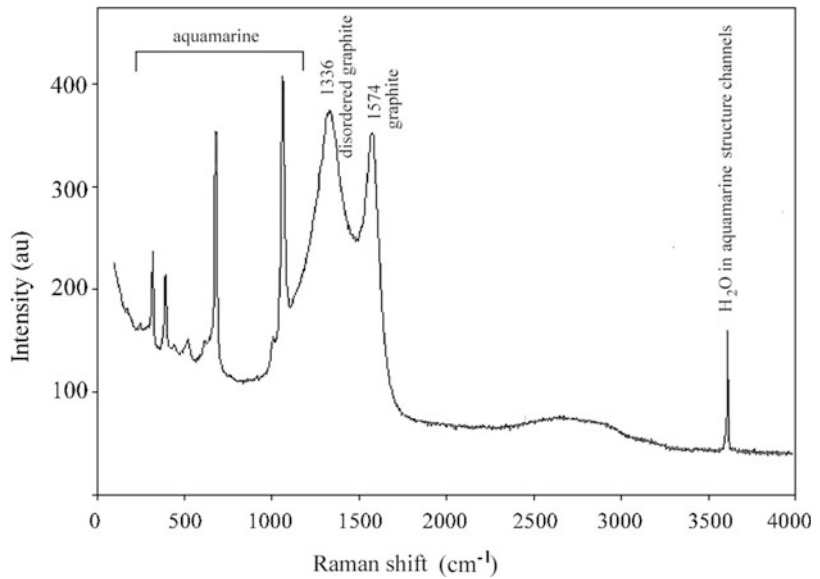


Fig. 3.15 Raman spectrum of a carbonaceous inclusion in aquamarine. The laser emission wavelength is 532 nm, the spectral resolution is 6 cm^{-1} , the laser power is 30 mW, and signal accumulation time is 120 s



3.2.4 Selection Rules

The Raman activity of normal modes is determined by changes of polarizability tensor components in corresponding vibrations. The magnitudes of the derivatives of the polarizability tensor components by normal coordinates determine the intensities of these vibrational modes and also form a second-rank symmetric tensor (so-called the Raman tensor) which is defined

for all point symmetry groups (see, e.g., Zhizhin et al. 1984; Kolesov 2018). Nonzero elements of the Raman tensor determine at which relative orientation of the crystallographic axes and the polarizations of the laser and scattered radiation vibrations of a given type of symmetry will be recorded in the Raman spectrum. Based on the Raman tensors, selection rules in Raman scattering for crystals, molecules, molecular groups, and ions are formulated.

For objects with C_{2v} symmetry, to which H_2O and H_2S molecules belong, vibrations of the symmetry types A_1 (symmetric stretching and bending vibrations) and B_1 (antisymmetric stretching vibrations) are permitted by the selection rules. Corresponding Raman bands of water molecules in the gas phase are observed at 3657, 1595, and 3756 cm^{-1} , respectively (Halonen and Carrington Jr 1988).

For isolated undistorted planar trigonal AB_3 ions (symmetry group D_{3h}) like CO_3^{2-} , NO_3^- , and BO_3^{3-} , symmetric stretching vibrations ν_1 with the symmetry A_1' as well as stretching (ν_3) and in-plane bending (ν_4) doubly degenerate vibrations of type E' are permitted in Raman spectra by the selection rules. Out-of-plane bending ν_2 vibrations with the symmetry A_2'' are prohibited.

For isolated tetrahedral AB_4 ions with the T_d symmetry (MoO_4^{2-} , AsO_4^{3-} , PO_4^{3-} , VO_4^{3-} , SO_4^{2-} , SiO_4^{4-} , etc.) in the Raman spectra the stretching ν_1 mode (with the A_1 symmetry), bending doubly degenerate ν_2 mode (with the E symmetry), and triply degenerate ν_3 stretching and ν_4 bending modes (with the F_2 symmetry) are allowed by the selection rules.

In real structures of minerals, the symmetry of tetrahedral ions decreases, sometimes to D_{2h} (flattened tetrahedron) or even to C_s , which leads to the removal of degeneracy and splitting of degenerate vibrations into separate components. To identify the scattering lines, one can use the known regularity established by different authors in numerous experimental studies: in most cases, the scattering lines corresponding to fully symmetric stretching vibrations have a smaller width and higher peak intensity than the scattering lines corresponding to degenerate vibrations. This empirical regularity is explained by the greater polarizability of bonds with fully symmetric stretching vibrations (Kolesov 2018).

Symmetry types of the vibrations of isolated complex ions may differ from that in crystals. For example, in calcite $CaCO_3$ having D_{3d} symmetry, CO_3^{2-} ions are located in positions on the third-order axis (D_3 positional symmetry) and do not change their symmetry compared to the free state. In this case, the same selection rules are valid as

for an isolated CO_3^{2-} ion. On the other hand, in aragonite (orthorhombic $CaCO_3$ polymorph with the D_{2h} symmetry), the crystal structure of which does not have axes of the third order, the positional symmetry of the CO_3^{2-} ion decreases to C_s , and according to the selection rules for the D_{2h} group, the out-of-plane bending mode (ν_2), which is classified as A_g , is active in the Raman spectrum of aragonite: corresponding band is observed at 853 cm^{-1} (Frech et al. 1980).

In vivianite $Fe_3^{2+}[PO_4]_2 \cdot 8H_2O$, which is monoclinic with the symmetry C_{2h} , there are no axes of the third order, and the symmetry of the phosphate ion also decreases as compared with isolated PO_4^{3-} . As a result, all vibrations are nondegenerate and are classified according to symmetry types as A_g , A_u , B_g , and B_u . In the Raman spectrum of vivianite, only A_g and B_g bands appear in accordance with the “alternative prohibition” rule applied to symmetry groups with an inversion center:

PO_4^{3-} in aqueous solution	PO_4^{3-} in vivianite
(Nakamoto 2009), cm^{-1}	(Piriou and Poullen 1984), cm^{-1}
$A_1 (\nu_1)$ 938	$A_g (\nu_1)$ 951
$E (\nu_2)$ 420	$A_g (\nu_2)$ 458; $B_g (\nu_2)$ 425
$F_2 (\nu_3)$ 1017	$A_g (\nu_3)$ 1053, 990; $B_g (\nu_3)$ 1018
$F_2 (\nu_4)$ 567	$A_g (\nu_4)$ 572, 539

For isolated regular octahedral AB_6 groups, ν_1 symmetric stretching mode with the symmetry A_{1g} , doubly degenerate ν_2 stretching mode with the symmetry E_g and triply degenerate ν_5 bending mode with the symmetry F_{2g} are permitted in the Raman spectra by the selection rules.

In accordance with the “alternative prohibition rule,” in IR spectra of isolated regular octahedral AB_6 groups, only the ν_3 stretching band and the ν_4 bending band (both having the F_{1u} symmetry) are observed. Anionic groups of this type [$Si(OH)_6$, $Al(OH)_6$, $Fe^{3+}(OH)_6$, $Mn^{4+}(OH)_6$, etc.] occur in the structures of ettringite-group minerals. In ettringite $Ca_6[Al(OH)_6]_2(SO_4)_3 \cdot 26H_2O$, the symmetry of which is C_{3v} , with triad axes and reflection planes being the only symmetry elements. As a result, the symmetry of the $[Al(OH)_6]^{3-}$ group

is also lowered. The ν_5 modes which were forbidden in the Raman spectrum according to the “alternative prohibition rule” for the free anion become nondegenerate and active. Vibrational modes of ettringite are classified according to the symmetry types A_1 , A_2 , and E . In accordance with the selection rules, only bands of A_1 and E vibrations appear in the Raman spectra (presumably, the bands at ~ 550 and ~ 345 cm^{-1} ; see Deb et al. 2003; Renaudin et al. 2007). Vibrations of type A_1 can be separately recorded under the conditions when polarizations of laser and scattered radiation and the C_3 crystallographic axis of a single crystal are parallel to each other.

The C_6 symmetry group of thaumasite $\text{Ca}_3[\text{Si}(\text{OH})_6](\text{SO}_4)(\text{CO}_3)\cdot 12\text{H}_2\text{O}$ contains axes of the second, third, and sixth orders. In accordance with this set of symmetry elements, the “alternative prohibition rule” becomes inapplicable, and the degeneration is removed from the triple degenerate modes. This leads to an increase in the number of possible scattering lines in the spectrum. In accordance with the table of group characters, in the spectra of structures with such symmetry, the existence of vibrational modes of the A , B , E_1 , and E_2 types is possible. In accordance with the selection rules and Raman scattering tensor, vibrations of symmetry types A , E_1 , and E_2 are active in the Raman spectra. The study of the polarized Raman spectra of a thaumasite single crystal showed that the fully symmetric vibrations of the $[\text{Si}(\text{OH})_6]^{2-}$ anion have a frequency of about 660 cm^{-1} (Kononov et al. 1990).

An example of the manifestation of the “alternative prohibition rule” is the absence of first-order Raman spectra in some minerals with inversion centers. Such minerals, for example, are halite NaCl and sylvite KCl having a cubic (O_h) symmetry. All atoms forming the structures of these minerals are located at the centers of inversion, and any displacements from their equilibrium positions violate the symmetry. As a result, the bands corresponding to all kinds of vibrations are forbidden in the first-order Raman spectra. However, with a large signal accumulation time, it is possible to record weak bands of the second order Raman spectra (Fig. 3.16). The selection rules for two-phonon spectra are determined using the tables

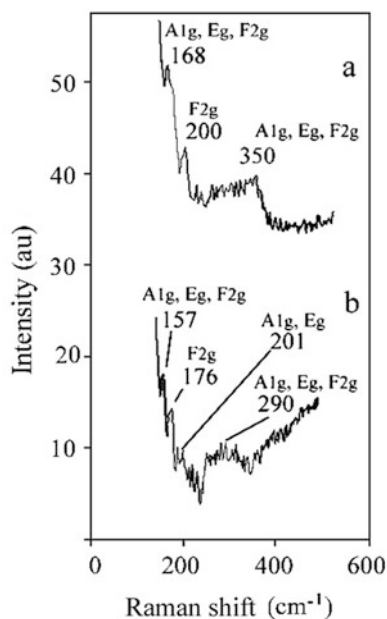


Fig. 3.16 Second-order Raman spectra of halite (a) and sylvite (b). The laser emission wavelength is 532 nm, the spectral resolution is 6 cm^{-1} , the laser power is 30 mW, and signal accumulation time is 200 and 25 s, respectively

of the characters of irreducible representations of the point group of the mineral under investigation. Thus, an analysis of the types of symmetry of two-phonon vibrations in crystals with a point group O_h shows that among the possible combination modes in this point group there are vibrations with symmetry types A_{1g} , E_g and F_{2g} , which are allowed in the Raman spectra. Consequently, second order Raman spectra can also be used for diagnostic purposes.

3.2.5 The Longitudinal-Transverse Splitting

The special feature of the Raman scattering method, which makes it difficult to interpret the spectra, includes the appearance of the longitudinal-transverse (LO - TO) splitting of lines in the spectra in crystals without an inversion center. In such crystals, some vibrations that are active in the Raman spectra are accompanied by changes in the dipole moment. As a result, vibrations of atoms lead to changes in the

macroscopic electric dipole moment in the crystal. The resulting additional electromagnetic field in turn affects the atoms. In the Raman spectra, such an interaction can result in the appearance of additional scattering lines. The *LO-TO* splitting theoretically exists in all cases when scattering occurs on dipole-active vibrations. A weak splitting results in changes of the shapes of some lines and appearance of additional shoulders. However, in crystals with the ionic character of bonds the magnitude of the *LO-TO* splitting can reach considerable values. For example, in the Raman spectrum of LiH, it is almost 500 cm^{-1} . In Raman spectra of molecular crystals, the splitting value only in some cases reaches 15 cm^{-1} (Zhizhin et al. 1984), but in most molecular crystals, the *LO-TO* splitting is not observed. The prediction of the *LO-TO* splitting in the spectra of the Raman spectra goes beyond the framework of factor group analysis.

In the case when a mineral without an inversion center has several dipole-active vibrations, several additional scattering lines may appear in the spectrum owing to splitting into *LO-TO* components (see, e.g., Raman spectrum of quartz in Fig. 3.11). As a result, the total number of lines in the spectrum may exceed the number of normal vibrations expected according to group theory. It should be noted that in the infrared absorption spectra, the frequencies of the longitudinal vibrations are not recorded, since only transverse vibrations are excited.

3.2.6 Orientation and Polarization Effects; Analysis of Water and OH Groups

A specific feature of Raman scattering is its tensor character. As a result, Raman spectra of single crystals depend on their orientation and the direction of polarization of the vector of the electrical component of the electromagnetic wave of laser radiation. Spectra obtained in different experimental geometries may differ from each other by the number of recorded scattering lines and their intensity (Fig. 3.17).

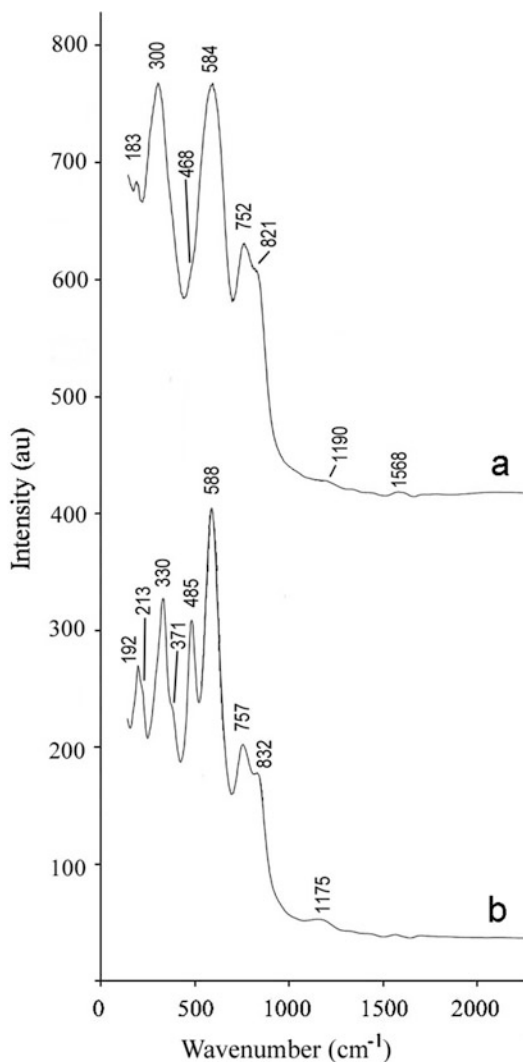


Fig. 3.17 Raman spectra of laachite $(\text{Ca,Mn})_2\text{Zr}_2\text{Nb}_2\text{TiFeO}_{14}$ (monoclinic, point group C_{2h}) obtained with the polarization of the laser beam parallel (upper curve) and perpendicular (lower curve) to the *a* axis of the crystal. The laser emission wavelength is 532 nm, the spectral resolution is 2 cm^{-1} , the laser power is 6 mW, and the focal spot diameter is about $15\text{ }\mu\text{m}$

With a random orientation of the single crystal, the scattering line intensities are also random. This uncertainty does not apply to spectra of powdery samples with chaotic orientation of microcrystals. A reproducible total spectrum averaged over all possible spatial orientations of the microcrystals can be obtained only if the size of the microcrystals in the powder is much less

than the diameter of the focal spot of the laser radiation. This mode of spectrum registration is most suitable for diagnostic purposes. In cases where it is impossible to prepare the powder, it is recommended to obtain several spectra at different orientations of the sample in order to select the most representative version of the spectrum.

Raman spectrum of a single crystal, obtained using polarized radiation, makes it possible to draw conclusions regarding the directions of chemical bonds relative to the crystallographic axes. This is especially important for determining the orientation of hydroxyl groups (e.g., in amphiboles, micas, tourmalines). Raman scattering is only possible if the electric field vector of an incident beam is not perpendicular to the O–H bond direction.

To study structural features of minerals, spectra of Raman spectra of single-crystal samples are taken. In such experiments, intensities of scattering lines depend on the mutual orientation of the crystallographic axes and on the directions of the polarization vectors of the incident and scattered radiation. In crystals with a tetragonal, hexagonal/trigonal, and cubic symmetry, it is possible to determine the type of symmetry of the vibrational mode of a group of equivalent coordinates based on polarized Raman spectra. In crystals having lower symmetry, polarization measurements make it possible to obtain information on the orientations of chemical bonds, since in some cases (especially in molecular crystals) polarization of some scattering lines depends on vibrations of single bonds (Kolesov 2018).

The polarizability of a bond in the longitudinal direction is much greater than in the transverse directions. Therefore, the scattering line corresponding to stretching vibrations of this bond is most intense when the polarization of the exciting laser radiation (and in the ideal case of the scattered light) coincides with the direction of this bond. This regularity can be illustrated by the example of micas. In phlogopite $\text{K}(\text{Mg}, \text{Fe}^{2+})_3[\text{AlSi}_3\text{O}_{10}](\text{OH}, \text{F})_2$ having monoclinic symmetry, OH groups coordinated by divalent octahedral cations are oriented almost parallel to the crystallographic c axis, perpendicular to the cleavage plane. The Raman scattering line at

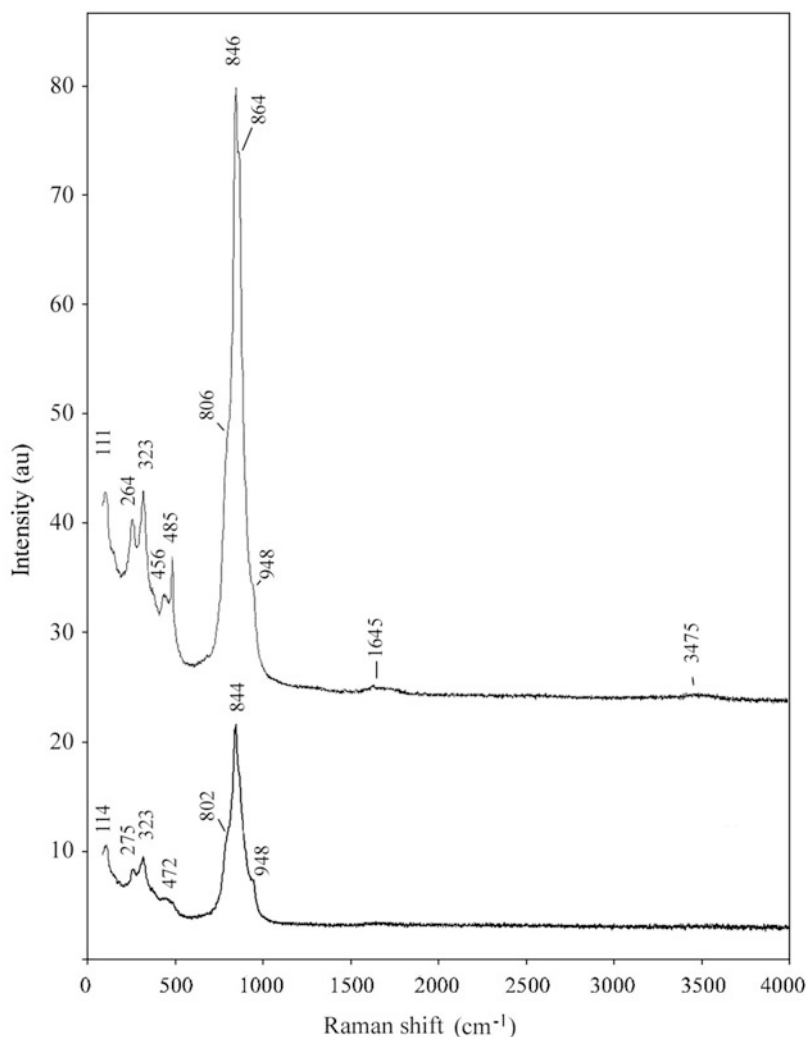
3709 cm^{-1} corresponding to stretching vibrations of hydroxyl groups has a maximum intensity when the polarization of laser radiation is perpendicular to the cleavage plane of the mineral sample, i.e., parallel to the c axis. A weak additional line at about 3666 cm^{-1} is observed in Raman spectra of phlogopite samples containing trivalent impurity ions, Fe^{3+} or Al^{3+} . Since the orientation of hydroxyl groups coordinated by trivalent cations deviates from the direction perpendicular to the cleavage plane, a weak scattering line can be recorded in the Raman spectra with polarization of laser radiation parallel to the cleavage plane. In muscovite $\text{KAl}_2[\text{AlSi}_3\text{O}_{10}](\text{OH})_2$, which is a dioctahedral mica, hydroxyl groups are almost parallel to the cleavage plane, and the band of stretching vibrations of OH groups (at 3628 cm^{-1}) has a maximum intensity in spectra excited by laser radiation with polarization parallel to the cleavage plane (Tlili et al. 1989).

Based on polarized spectra of tourmaline group minerals, it was found that the OH groups are mainly oriented along the threefold c crystallographic axis (Gasharova et al. 1997; Berryman et al. 2016). Polarized Raman spectra of the orthorhombic mineral magnesiochlorophane $\text{MgAl}_2\text{Si}_2\text{O}_6(\text{OH})_4$ revealed the presence of three OH groups, one of which is oriented almost perpendicular to the c axis (Fuchs et al. 2001).

In some cases, the orientation of complex anionic groups can be determined from polarized Raman spectra. Based on the data obtained for a columnar thaumasite crystal, Kononov et al. (1990) have confirmed that almost flat CO_3^{2-} group (Edge and Taylor 1971) is oriented perpendicular to the C_6 axis of the crystal.

Raman spectroscopy has a low sensitivity in determination of water in minerals. The H_2O molecule has a weak polarizability and, as a result, a weak response to excitation radiation. Bands of O–H-stretching vibrations are usually observed in the range from 3000 to 3800 cm^{-1} , but bands of acidic OH groups and very strong hydrogen bonds may have Raman shifts below 3000 cm^{-1} . In most cases, bands of H–O–H bending vibrations of H_2O molecules are observed in the range 1600 – 1700 cm^{-1} , but with a low water content, these bands are recorded with difficulty and only with a successful selection of

Fig. 3.18 Raman spectra of martyite $\text{Zn}_3(\text{V}_2\text{O}_7)(\text{OH})_2 \cdot 2\text{H}_2\text{O}$ obtained at the laser emission wavelength of 532 nm, the spectral resolution of 2 cm^{-1} , the laser power of 4 and 13 mW, and the signal accumulation time of 200 and 50 s (for the upper and lower curves, respectively)



experimental conditions. An increase in the accumulation time at a given laser power or an increase in the laser power may lead to local overheating and dehydration of the sample (see Fig. 3.18).

In the structure of fluorapophyllite-(K), water molecules occupying a single crystallographic position are asymmetric: the positional symmetry of H_2O decreases to C_1 , and the hydrogen atoms belonging to the same molecule are nonequivalent. A significant difference in the interactions of the two hydrogen atoms with their nearest environment leads to the fact that stretching vibrations

of OH bonds in the water molecule are practically independent (Ryskin and Stavitskaya 1990). The broad band with a maximum of about 3013 cm^{-1} and the narrow band at 3564 cm^{-1} refer to the stretching vibrations of OH bonds, which form strong and very weak hydrogen bonds, respectively (Fig. 3.19).

In the structure of hydroxylapophyllite-(K), both asymmetric H_2O molecules and OH groups are present. The broad band at about 2990 cm^{-1} and the narrow band at 3569 cm^{-1} correspond to a strong and a weak hydrogen bonds formed by H_2O , respectively. Another narrow band (with a

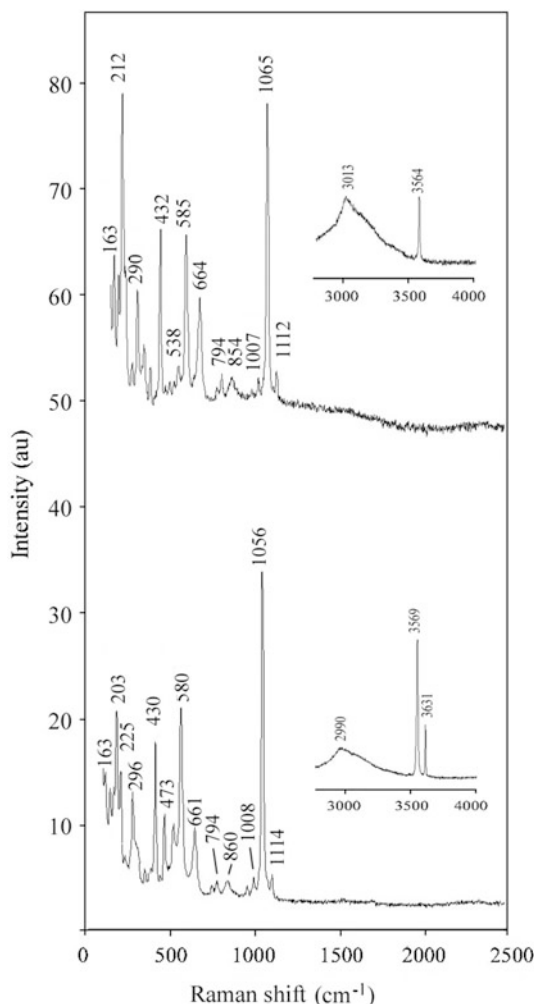


Fig. 3.19 Raman spectra of fluorapophyllite-(K) $\text{KCa}_4[\text{Si}_8\text{O}_{20}]\text{F}\cdot 8\text{H}_2\text{O}$ (upper curve) and hydroxylapophyllite-(K) $\text{KCa}_4[\text{Si}_8\text{O}_{20}](\text{OH})\cdot 8\text{H}_2\text{O}$ (lower curve) obtained using 532 nm laser radiation

half-width of about 3 cm^{-1}) is observed at 3631 cm^{-1} and corresponds to stretching vibrations of the OH group.

In some cases when the number of hydrogen-containing groups in the mineral is insignificant, the Raman spectroscopy method does not allow one to unambiguously distinguish between water and hydroxyl groups. In such cases, it is more appropriate to use infrared absorption spectroscopy.

3.2.7 Effect of Luminescence

Emission of photoluminescence excited by the laser beam is a serious problem of Raman spectroscopy of minerals. Usually, luminescence is observed as broad bands superimposed on the Raman scattering spectrum (Fig. 3.20, upper curve). The intensity of luminescence can be many times (up to 10^3 – 10^4) greater than the intensity of the Raman signal, which prevents the registration of a high-quality spectrum or even makes it impossible to obtain Raman spectrum at all.

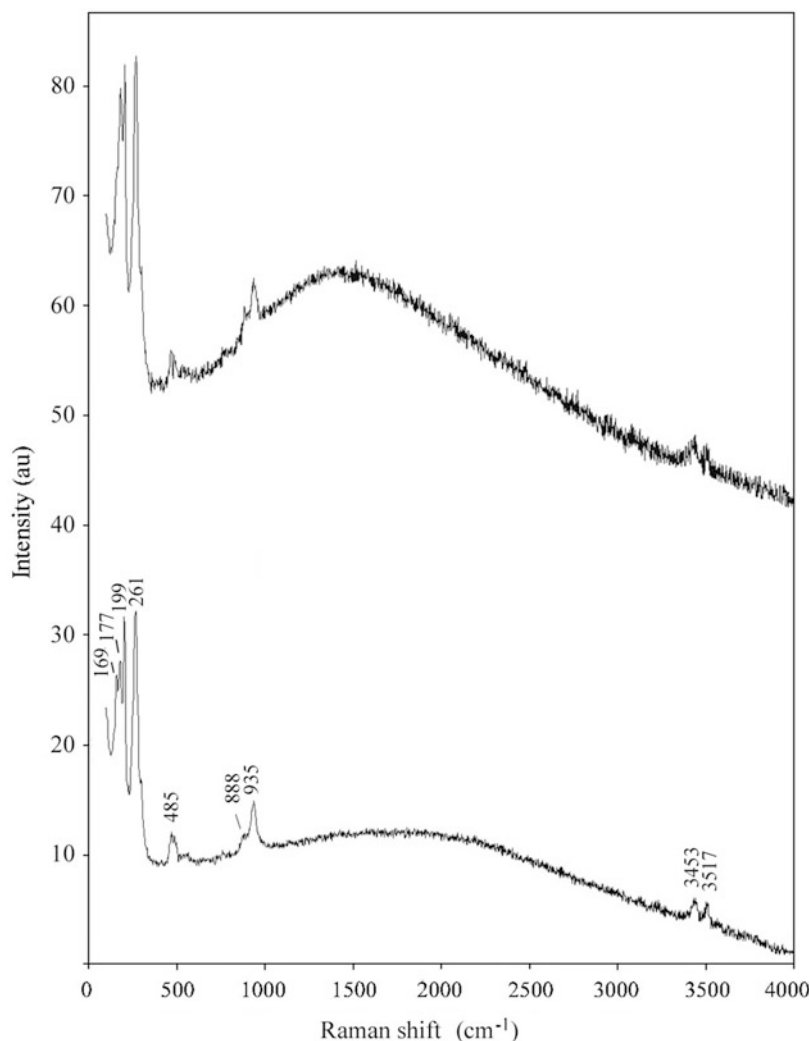
The main cause of luminescence is the coincidence of the frequency of the exciting laser radiation with the frequencies of electronic transitions of the luminescent center in the mineral. The most effective way to eliminate luminescence is the use of laser radiation with a longer wavelength λ_{exc} , the photon energy of which is insufficient to excite electronic energy levels. Unfortunately, with increasing wavelength of laser radiation, the intensity of the useful Raman signal I_R decreases significantly according to the law $I_R \sim \lambda_{\text{exc}}^{-4}$. In such situations, long-time accumulation of the useful signal leads to an improvement in the signal-to-noise ratio (Fig. 3.20, lower curve).

In cases when it is not possible to eliminate the luminescence, one can resort to recording several spectra using lasers with different wavelengths. For each type of radiation, the spectral luminescence lines appear in a specific spectral range. The bands that will be present with a constant frequency in the spectra obtained at different wavelengths of the exciting radiation should be referred to the lines of Raman scattering.

3.2.8 Destructive Effect of Laser Radiation

Local temperature increase due to strong absorption of laser radiation may result in alteration or decomposition of the sample. In the Raman microprobe analysis this problem is especially

Fig. 3.20 Raman spectra of an unoriented sample of romanorlovite $\text{K}_8\text{Cu}_6\text{Cl}_{17}(\text{OH})_3$ obtained at the laser emission wavelength of 532 nm, the spectral resolution of 6 cm^{-1} , the laser power of 3 and 1.5 mW, and the signal accumulation time of 4 and 17 min (for the upper and lower curves, respectively)



significant. Therefore, the selection of conditions for a nondestructive experiment plays an extremely important role in experiments on Raman scattering.

Special attention should be paid to proper selection of laser power when working with highly colored or opaque minerals, which include most sulfides and sulfosalts. Dark coloring of minerals causes a strong absorption of exciting radiation, which results in attenuation of scattered signal. To enhance the intensity of the Raman signal, an increase in the laser pump power is required. However, it should be borne in mind

that increasing the power of laser radiation leads to an increase in the energy absorbed by the mineral. Since most minerals have relatively low thermal conductivity, the absorbed energy causes a local increase in temperature in the focal volume of the laser beam. Too high laser power can result in local thermal destruction of the mineral structure, leading to the formation of cavities on the sample surface (Figs. 3.21 and 3.22) or cavities with a destroyed structure inside the sample. However, in most cases optimizing the experimental conditions (reducing the laser excitation power and increasing the signal accumulation

Fig. 3.21 Caverns formed on the surface of melanarsite at a laser power of 13 mW and laser wavelength of 532 nm, focal spot diameter of $\sim 15 \mu\text{m}$, and signal accumulation time of 10 s

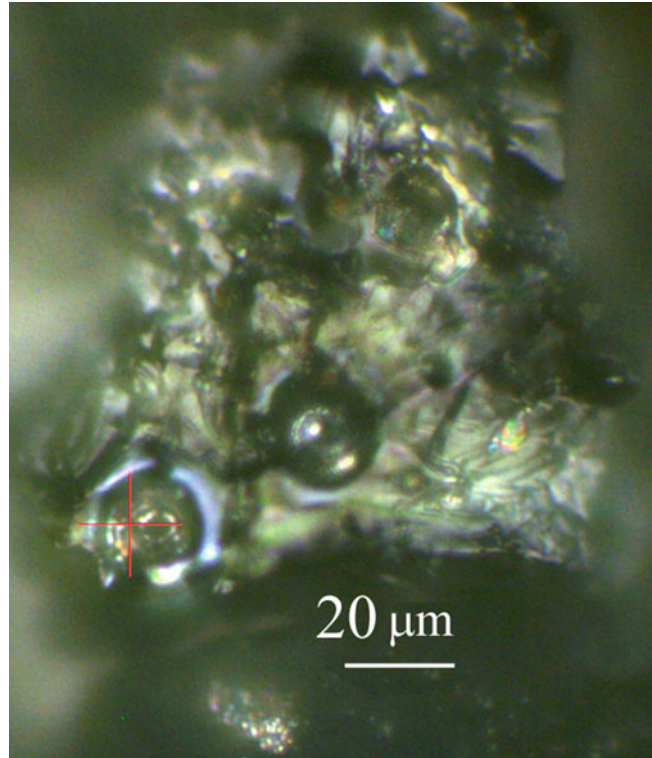
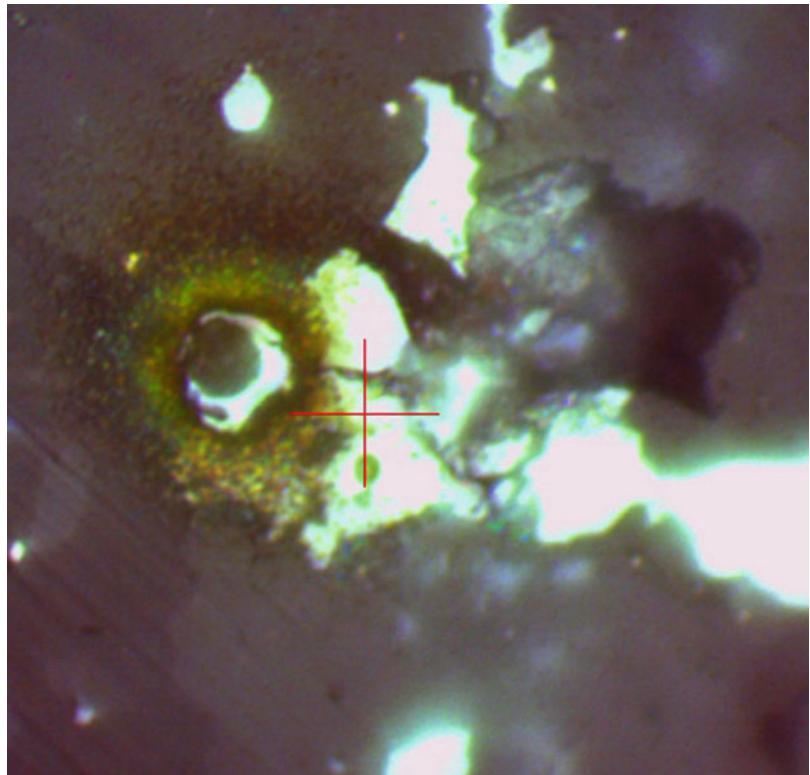


Fig. 3.22 The thermal destruction zone formed on the surface of a crystal of vorontsovite (Hg_5Cu) $\text{TlAs}_4\text{S}_{12}$ at a laser power of 1.5 mW and laser wavelength of 532 nm, focal spot diameter of $\sim 15 \mu\text{m}$, and signal accumulation time of 1 h. Field width $100 \mu\text{m}$. It was not possible to obtain Raman spectrum of the mineral due to its thermal instability



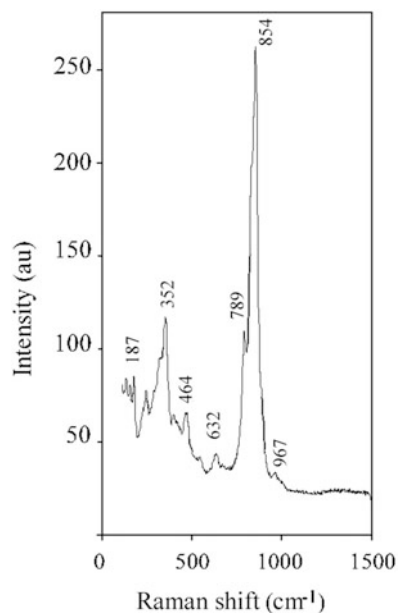


Fig. 3.23 Raman spectrum of melanarsite $K_3Cu_7Fe^{3+}O_4(AsO_4)_4$ obtained at the laser emission wavelength of 532 nm, spectral resolution of 6 cm^{-1} , laser power of 4 mW, focal spot diameter of $\sim 15\text{ }\mu\text{m}$, and signal accumulation time of 100 s

time) makes it possible to obtain scattering spectra even on thermally unstable samples (Fig. 3.23).

In some cases, it is possible to reduce the degree of overheating by placing microscopic mineral samples on a metal substrate, which leads to acceleration of the heat sink. The correct sequence of actions when working with an unknown colored opaque or especially valuable sample is the use of low-power laser source at the initial stage of research. A gradual increase in power with constant monitoring of the state of the sample will prevent its damage or destruction. To improve the quality of the Raman spectra at low power of the exciting radiation, an increase in the time of accumulation of the Raman signal may play a positive role.

Additional information on the practical application of Raman spectroscopy can be obtained from numerous books and review articles (Reshetnyak and Bukanov 1991; Nasdala et al. 2004; Larkin 2011; Vandenabeele 2013; Kolesov 2018).